ISSN: 2688-8645

Prediction and Analysis of End Milling Deformation of Casing Parts Based on Quasi-Static Mechanics

Huan Zhao [1], Teng Hu [1, 2], Sijia Peng [1], Zichun Ma [1]

[1] Southwest Petroleum University, Chengdu Sichuan, 610500, China

[2] Sichuan Science and Technology Resource Sharing Service Platform of Oil and Gas Equipment Technology, Chengdu Sichuan, 610500, China

Abstract

In view of the deformation generated during the casing end milling process, the casing parts are meshed and nodaled through Hypermesh, and the finite element simulation software ABAQUS is developed for secondary development by Python, so as to realize the simulation process of quasi static outer ring belt end milling. Combined with the simulation results, the deformation law in the process of casing end milling is analyzed, and the maximum deformation is near the machining position, and the deformation gradually decreases as it moves away from the machining position; the local geometric characteristics of the casing will lead to significant inconsistencies in the milling deformation of the ring belt end. The average errors predicted by the simulation model in the local height and feed direction are 13.66% and 12.17%, respectively, and the average error and maximum error of the overall prediction of the model are 19.75% and 14.28%, respectively, which are less than 20%, and the prediction accuracy is within the acceptable range, which shows the reliability of the simulation model. Using the simulation model, the factors affecting the milling deformation of the casing end are studied, which provides guidance for the future research of the end milling deformation compensation technology.

Keywords

Quasi Static; Casing; End Milling; Deformation; Prediction.

1. Introduction

As one of the key components of aero-engines, the casing is a typical thin-walled component with weak rigidity [1]. This makes the casing prone to "tool deflection" during milling, meaning there is a deviation between the actual and theoretical milling amount, which directly affects the machining accuracy of the workpiece. In order to reduce machining errors, it is necessary to study the deformation generated during the milling process of turbine casings, explore efficient and high-precision prediction methods for milling deformation of aero-engine casings, and analyze the influencing factors of casing milling deformation on this basis. This will provide theoretical and data support for future research on casing milling deformation compensation technology and has important engineering value.

Regarding the machining deformation of thin-walled parts, J.W. Sutherland and R.E. Devor[2] proposed a theoretical method for calculating the relationship between the deformation of milling tools and the thickness of the undeformed shoulder in the instantaneous milling process, as well as the surface error of the workpiece. M.R. Lajczok[3] first introduced finite element technology into the field of metal cutting and conducted in-depth research and analysis on the cutting mechanism. E.Budak and Y. Altintas[4] studied the milling deformation of thin-walled parts and used the finite element method to predict its deformation. MA[5] used finite element simulation technology to predict the deformation and law generated when side milling thin-

ISSN: 2688-8645

walled parts. Ratchev S[6] and others studied the machining deformation prediction method and compensation correction technology for weak stiffness parts, combined neural network method and genetic algorithm to establish a dynamic model of cutting force, and loaded the cutting force load into the finite element model of the milling process, which well predicted the machining deformation of thin-walled parts during the milling process. Hua[7] obtained experimental data by designing orthogonal experiments and established a milling deformation prediction model for thin-walled parts based on BP neural network using the experimental data. In China, Liao Kai[8] studied the stress distribution generated after the processing of aluminum alloy thin-walled parts, constructed an analytical model of stress-deformation of aluminum alloy thin-walled parts, and completed the uncertain calculation of the processing deformation of thin-walled parts; Li Tong[9] studied the influence of processing position and milling parameters on the processing deformation of thin-walled parts during the milling process of titanium alloy bent thin-walled parts, and successfully predicted the position of the maximum deformation; Lou Wenming[10] adopted a simulation prediction method that considered the coupling effect of tool/workpiece deformation, material removal effect and the change of milling force loading point caused by workpiece deformation, established a finite element analysis model for the prediction of the processing deformation of thin-walled parts, and conducted a study on the deformation of thin-walled parts. The deformation prediction and experimental verification of the milling of the aerospace titanium alloy frame workpiece were carried out. The simulation results were in good agreement with the experimental data. Yu Jin [11] used empirical formulas to obtain the magnitude of the cutting force during the cutting process, edited the dynamic machining script of the cutting force using Python language, and realized the deformation prediction of the cutting of large curved thin-walled parts through the static implicit module of the simulation software ABAQUS. Zhang Yu [12] used the finite element simulation software ANSYS to establish a static implicit milling model of thin-walled parts, analyzed the deformation of thin-walled parts at different lengths and heights during the side milling process, and obtained the deformation law at different positions.

It is easy to see that existing research has three main limitations. First, domestic and international scholars mostly employ dynamic or static methods when studying the machining deformation of thin-walled parts. However, due to the large size of the casing and limited computational resources, dynamic methods suffer from efficiency and cost issues. On the other hand, static methods, in order to improve computational efficiency, often simplify the machining of thin-walled casings, failing to fully consider the impact of material removal on component rigidity and neglecting the influence of numerous local features on the casing on machining deformation, leading to accuracy and reliability issues. Furthermore, previous studies have mostly focused on side milling, with relatively little research on end milling, while casing parts have many thin-walled features requiring end milling.

Therefore, this study focuses on the deformation of end milling of casing parts. Based on quasi-static analysis, Hypermesh is used to mesh and number the parts. ABAQUS is then further developed using Python to establish a reliable simulation model for end milling of the casing. Based on this model, a method for predicting the deformation of the outer ring belt during end milling of the casing is studied. Furthermore, the influencing factors of deformation and their weight ratios are analyzed.

2. Deformation Simulation Model Establishment and Verification

2.1. Deformation Mechanism and Quasi-Static Analysis Process of End Milling for Thin-Walled Parts

As shown in Figure 1, due to the low stiffness of thin-walled parts and the good stiffness of the cutting tool, during end milling, the cutting tool squeezes the thin-walled parts under the action

ISSN: 2688-8645

of milling force, causing elastic deformation, which causes the theoretical machining plane to shift along the direction of the cutting tool axis, and the actual milling amount cannot reach the theoretical milling amount; after the milling is completed, the elastic deformation of the thin-walled parts recovers, thus causing the actual wall thickness to be greater than the theoretical wall thickness. This is the "tool deflection" phenomenon, which is the main reason for the machining error of thin-walled parts [6].

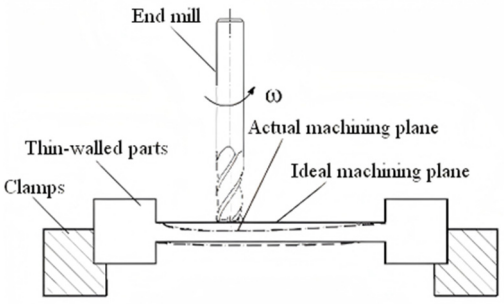

Figure 1. Schematic diagram of end milling cutter for thin-walled parts

Quasi-statics is a mechanical analysis method that lies between dynamics and statics. It discretizes the dynamic process of a system and uses the instantaneous static characteristics of the system to approximate its dynamic behavior, aiming to maximize both computational accuracy and efficiency. In terms of the application of quasi-statics, Jones[13] first proposed a quasi-static analysis model for ball bearings. In recent years, scholars such as Ohta[14], Li X H[15], Yu Dong[16], Yu Jie[17], Chen Yinglin[18], and Gao Feng[19] have used quasi-statics for the dynamic analysis of bearings. However, few scholars use quasi-statics analysis in the milling process.

The overall technical route for the casing end milling deformation analysis based on quasi-statics is shown in Figure 2. The quasi-statics process discretizes the dynamic milling process into several analysis steps. Within any time step, the stress analysis and static deformation calculation of the thin-walled part are performed. Then, the cutting parameters are used to "kill the unit" to achieve the purpose of material removal. After the material is removed in each analysis step, the stiffness of the thin-walled part decreases. At this time, the stress analysis and static deformation calculation of the thin-walled part are performed again.

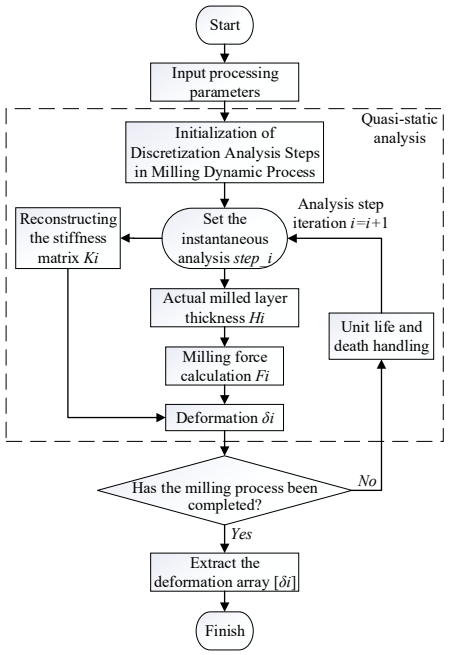

Figure 2. Overall technical route

ISSN: 2688-8645

2.2. Establishment of a Casing End Milling Deformation Model based on Quasi-Statics

2.2.1. CAD Model Building and Material Properties

(1) CAD modeling of casing

Simulation was performed on the end milling of the outer ring band on the surface of a large aircraft casing. The outer surface of the casing has "oil pipe" interface platforms. In order to realistically reflect the milling process of the casing, SIEMENS NX was used to create a one-to-one model of the casing based on the actual object. All features of the outer surface of the casing were preserved, as shown in Figure 3. Taking the end milling of the outer ring band on the casing surface as an example, the vertical height of the surface is 54 mm and the wall thickness is 5 mm.

Figure 3. Turbine casing model

(2) Mesh division and numbering of casing parts

The quality of mesh generation directly affects the simulation accuracy of finite element method [20]. The casing model has a complex structure, and it is difficult to directly perform mesh generation using ABAQUS software. Therefore, the casing mesh is generated using the professional mesh generation software Hypermesh. At the unprocessed location, there are many local features, so tetrahedral meshes are used for generation; while for the processed location, i.e., the outer ring, hexahedral meshes are used to ensure the quality of the mesh, the efficiency of the calculation, and the accuracy of the results, which is conducive to the calculation. A total of 211,745 meshes are generated.

In order to realize the movement of the load in the simulation and simulate the material removal effect in the actual milling process, it is necessary to number the element nodes at the processing location, and at the same time, to separately divide and establish sets for the corresponding elements; therefore, Hypermesh is used to number the elements to facilitate the subsequent establishment of the local coordinate system and to delete the elements using the birth and death element technique.

(3) Material properties

The casing of this type of aero-engine is made of high-temperature alloy GH4169, with mechanical properties [21]: density 8470 kg/m3, elastic modulus 206 E/GPa, and Poisson's ratio 0.3 μ.

During the casing milling simulation, the material constitutive model describes the influence of strain rate and strain on the material flow stress during milling. Therefore, in order to truly reflect the characteristics of the processed material and simulate the deformation of the material under load, the Johnson-Cook constitutive model, which is widely used in cutting simulation, is selected [22]. By consulting relevant literature, it can be found that the correlation coefficient of GH4169 material in the Johnson-Cook constitutive model is [23]: A=980, B=1370, n=0.02, C=0.164, m=1.03.

(4) Unit life and death

According to the actual milling process, nodes at the processing positions are created into corresponding sets according to the milling positions and sequences. The corresponding units

ISSN: 2688-8645

are "killed" step by step using the "unit birth and death technique" to complete the simulation of milling. Here, killing a unit does not mean removing the unit from the workpiece, but multiplying the unit matrix by a small scaling factor, as shown in Equation (1) [10]:

$$KU = F \tag{1}$$

In the formula, — stiffness matrix, typically taken as 10e-6; — displacement matrix of the corresponding node; — load matrix of the element.

After "killing" the elements, all properties of these elements are close to zero and do not participate in subsequent calculations. The "killed" elements will not be displayed in the software, allowing the stiffness of the entire workpiece to change as the machining process progresses, just like in actual milling, conveniently simulating the material removal process in casing milling.

2.2.2. Load Application and Boundary Conditions

In order to simulate the end milling process of the casing parts, the effect of the tool on the casing is equivalent to the effect of the instantaneous milling force on the workpiece in the simulation. In order to demonstrate the effect of the milling force during the milling process and simplify the analysis process of the entire simulation, the milling force load is applied to the node of the machining surface according to the principle of static equivalence [20]. The milling force is applied by applying axial, tangential and radial three-way milling force loads to the node.

As can be seen from the principle of quasi-static analysis, dynamic explicit analysis is decomposed into many static implicit analyses. If each static implicit analysis step is established manually, it will greatly increase the workload. At the same time, each node needs to establish a local coordinate system, which is prone to errors if done manually. Therefore, through the Python secondary development interface of ABAQUS, Python scripts are compiled to realize the establishment of quasi-static analysis steps and local coordinate systems, and to complete the functions of load "loading, unloading, and element birth and death", so as to achieve the purpose of simulation of milling of aero-engine casing.

(1) Establishment of a local coordinate system

The aero-engine casing is a large rotating body. The direction of the load on each node at each position changes with the position. Therefore, the main idea of establishing a local coordinate system by compiling Python code is to establish two direction vectors based on the node coordinates, through the global coordinate system, one representing the tool feed direction and the other representing the tool axis. Finally, a local Cartesian coordinate system is established according to the "right-hand rule".

(2) Analysis step establishment and cell birth/death settings

To achieve the process of "milling force loading, deformation solution construction, and element birth and death setting", an analysis step needs to be established for each element set. This simulation is a static analysis, and the analysis step type is Static General. In each static analysis step, the corresponding "birth and death elements" are set to delete the elements.

(3) Boundary condition setting

Considering the characteristics of the studied casing as a large rotating thin-walled part, clamping plates are used in actual processing. The casing is fixed by clamping the flange at the bottom. In actual processing, eight clamping plates are evenly distributed at the bottom of the casing to clamp the workpiece. Therefore, the end face of the bottom of the casing part is divided into eight parts for full constraint, as shown in Figure 4. The width of each constraint is 60 mm, which is consistent with the width of the clamping plates in actual processing.

ISSN: 2688-8645

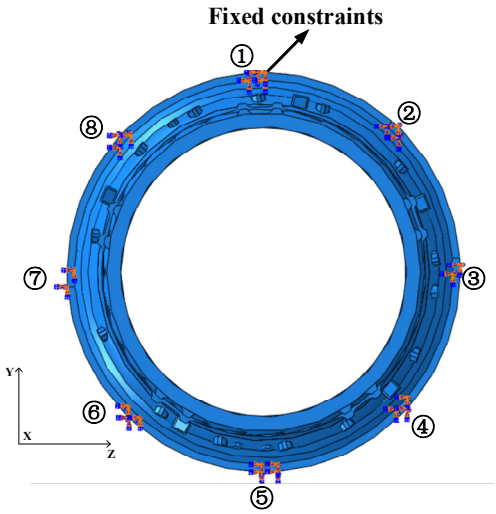

Figure 4. Schematic diagram of casing boundary condition settings

3. Examples and Verification

3.1. Simulation Calculation

Based on the previously established simulation model of the aero-engine casing end milling, the solution is obtained after quasi-static processing. According to the actual machining process, full-tooth milling is selected, with milling parameters , , and . Figure 5 shows the casing machining deformation cloud diagram during the machining process.

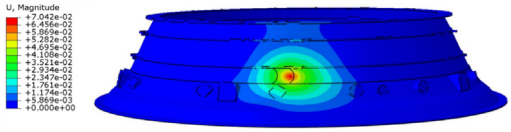

Figure 5. Simulated deformation cloud map of the casing

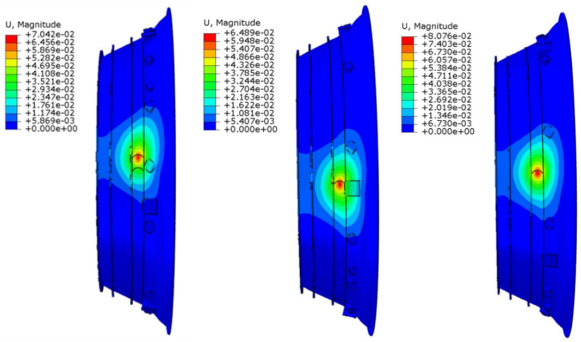

(a) Near a smaller pipeline platform (b) Near a larger pipeline platform (c) Not near a pipeline platform

Figure 6. Deformation contour plots at different locations in the simulation

As can be seen from the deformation cloud diagram, the maximum deformation is near the machining position, and the deformation gradually decreases as it moves away from the machining position. From the machining position downwards, due to the bottom of the casing being close to the fixed constraint end, plus the presence of the oil pipeline platform in the lower part of the machining area, the stiffness of the casing is greater and the deformation is smaller as it gets closer to the bottom. From the machining position upwards, the deformation is smaller

ISSN: 2688-8645

as it moves away from the machining position, and the deformation influence range becomes smaller as it gets closer to the top of the casing. This is mainly due to two reasons: (1) There is a radial rib structure on the outer surface from the machining position upwards to the top of the casing, plus the end face of the top of the casing, which makes the stiffness of the casing greater as it goes up, and the amount of deformation and the deformation influence range also decrease. (2) The casing parts are conical, and the diameter of the casing is smaller as it gets closer to the top, which leads to an increase in stiffness and a corresponding decrease in the amount of deformation and the deformation influence range.

Figure 6 shows the deformation contour maps when milling the casing at different positions. As can be seen from the figure, the maximum deformation occurs at the milling position, and the distribution of the deformation contour maps is similar across different milling positions. The only difference is the magnitude of the deformation. Due to the complex structure of the casing, the oil supply pipe platform at the bottom of the milling position is relatively close to the milling position. The oil supply pipe platform has a blocky structure with a large thickness and uneven distribution, significantly affecting the local stiffness at the milling position. The size of the oil supply pipe platform also affects the deformation; smaller oil supply pipe platforms have less impact on structural stiffness than larger ones, and the closer to a larger oil supply pipe platform, the smaller the deformation. In summary, the analysis of the contour maps shows that the simulation results are consistent with the structural characteristics of the casing, demonstrating the rationality of the simulation and its value.

3.2. Experimental Verification

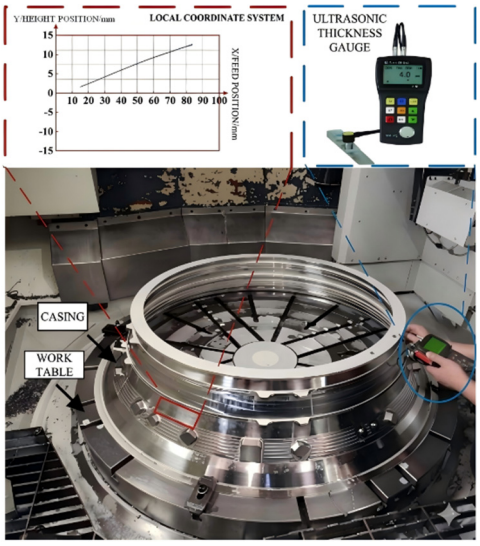

Figure 7. Schematic diagram of deformation measurement in experiments and simulations

To verify the accuracy and reliability of the simulation results, an end milling experiment of an aero-engine casing was conducted. The machining deformation perpendicular to the surface of the machining ring was compared and verified from both local and global perspectives. The experiment was conducted at the XX casing factory; due to confidentiality requirements, specific photos of the experimental site cannot be shown. The end milling of the casing was performed on a five-axis machining center, using milling parameters consistent with the simulation. After milling, an ultrasonic thickness gauge was used to measure the machining deformation perpendicular to the surface of the machining ring, as shown in Figure 7. Taking 1/36 of the entire casing (approximately 100 mm arc length), i.e., the red portion in the figure, a coordinate system was established with the midpoint of the machining position in the height direction as the origin. On the straight line x=0 in the height direction, at 5 mm intervals, the deformation at each point within a 15 mm range above and below the midpoint of the

ISSN: 2688-8645

coordinate axis was compared. Similarly, on the straight line y=0 in the feed direction, starting from the origin of the coordinate axis, the deformation at each point within a 100 mm range in the positive x direction was compared at 10 mm intervals.

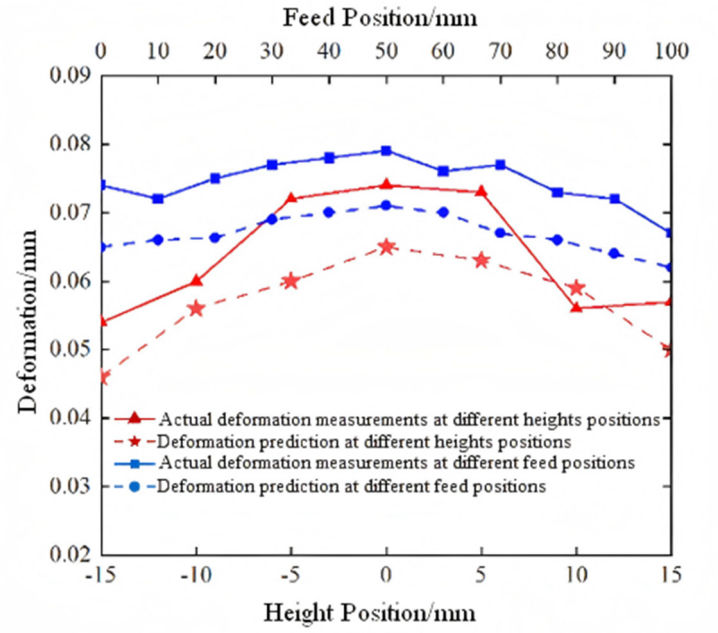

Figure 8. Comparison of verification results in local height and feed directions.

As shown in Figure 8, the predicted and measured deformation values are roughly consistent with the deformation trends of the casing along the surface height and feed direction of the ring belt. In the height direction, the overall deformation trend is generally larger in the middle and smaller at the edges. This is because there is a rib structure above the machining area, and as the height increases, the casing diameter decreases. The combined effect of these two factors results in greater casing stiffness and smaller deformation as the casing moves further away from the origin of the coordinate axis upwards. Downwards from the middle machining position, while machining ribs are also present, the stiffness increases further away from the origin of the coordinate axis due to the proximity to the oil supply pipe platform and bottom constraints, resulting in smaller deformation. In the feed direction, the deformation still shows a general trend of larger deformation in the middle and smaller deformation at the edges. This trend is due to the presence of the two bottom oil supply pipe platforms. The relatively large thickness of the oil supply pipe platforms has a certain impact on the local stiffness, resulting in smaller deformation at the ends closer to the "oil supply pipe platforms" and larger deformation in the middle, further away from the platforms.

Meanwhile, analysis of the deformation shows that the average error of the simulation model in the height direction is 13.66%, and the average error in the feed direction is 12.17%. This indicates that, at local locations, the simulation model can accurately predict the deformation trend and amount of the casing during machining.

To verify the global simulation results of the casing, the middle position of the machining area, i.e., the y=0 position in the local coordinate system, was selected, and 18 points were taken on the casing at 20° intervals for verification, as shown in Figure 9.

The comparison between experimental and simulated values at each node is shown in Table 1 above. Analysis reveals an average relative error of 14.28% and a maximum relative error of 19.75%. Errors between the two are unavoidable. The main reasons for these errors are as follows:

ISSN: 2688-8645

(1) Milling force loading: This paper uses a static implicit solver simulation method to dynamically load the load. The applied load is a three-dimensional average load. In actual machining, the milling force fluctuates, leading to errors between the two and resulting in prediction errors.

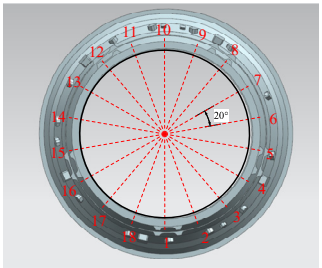

Figure 9. Schematic diagram of global verification location

Table 1. Comparison of experimental and simulated values

Node number	Experimental values	Simulation values	relative error	Node number	Experimental values	Simulation values	relative error
1	0.071	0.062	12.68%	10	0.053	0.061	15.09%
2	0.079	0.066	16.46%	11	0.088	0.071	19.32%
3	0.079	0.071	10.13%	12	0.081	0.065	19.75%
4	0.080	0.065	18.75%	13	0.077	0.063	18.18%
5	0.068	0.058	14.71%	14	0.075	0.065	13.33%
6	0.084	0.074	11.90%	15	0.083	0.068	18.07%
7	0.079	0.073	7.59%	16	0.078	0.066	15.38%
8	0.051	0.059	15.69%	17	0.090	0.079	12.22%
9	0.071	0.063	11.27%	18	0.061	0.057	6.56%

(2) Vibration generated during machining: As discussed in Chapter 2, high-temperature alloys are difficult-to-machine materials, and corresponding vibrations may occur during actual machining. The simulation did not consider the influence of vibration, leading to errors.

(3) Tool wear: Although the tool life is extremely short during machining, and the tool wear is very small, greatly reducing the impact of tool wear, the wear still exists. This was ignored in the study.

(4) Measurement error: The casing is relatively large, while the machining deformation of the casing is relatively small, inevitably leading to measurement errors.

Based on the above analysis, the error between simulation and experiment is unavoidable. However, the comparison shows that the average error of 14.28% and the maximum error of 19.75% predicted by the simulation model are both less than 20%. Compared with the average error and maximum error in similar studies [10][25], the prediction accuracy is within an acceptable range. Considering the combined effects of other actual factors and errors, it shows that the error caused by the above series of factors is within an acceptable range. The simulation model can effectively predict the deformation of the casing end milling process.

3.3. Analysis of Influencing Factors

Theoretical research combined with practical experience reveals that many factors influence machining deformation. This study primarily focuses on milling parameters and the number of clamping plates. To investigate their impact on casing machining deformation, a simulation model validated through experiments is used as a basis to study the maximum machining deformation of the casing under different milling parameters and different numbers of

ISSN: 2688-8645

clamping plates, exploring the influence law of casing deformation. Figure 10 below shows a comparison of deformation when other influencing factors remain constant, with different values of a certain factor.

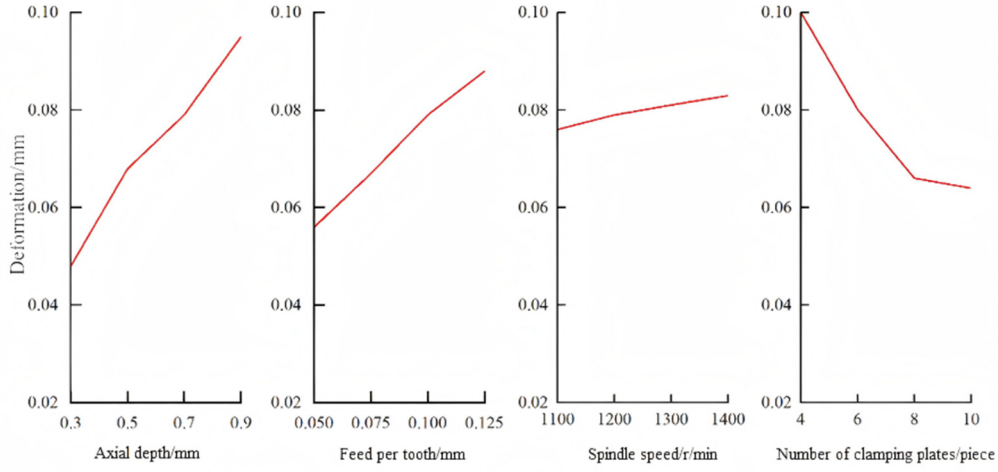

Figure 10. Influence curves of different factors on deformation

Figure 10(a) shows a feed per tooth of 0.1 mm/z, a spindle speed of 1200 r/min, and axial depths of cut of 0.3 mm, 0.5 mm, 0.7 mm, and 0.9 mm. As can be seen from the figure, the machining deformation of the housing increases with the increase of the axial depth of cut, indicating that the axial depth of cut has a significant impact on the machining deformation of the housing. Figure 10(b) shows an axial depth of cut of 0.7 mm/z, a spindle speed of 1200 r/min, and feed per tooth values of 0.05 mm/z, 0.075 mm/z, 0.1 mm/z, and 0.125 mm/z. As shown in the figures, the machining deformation of the housing increases with the increase of feed per tooth, but the impact is not as significant as that of the axial depth of cut. For example, in Figure 10(c), the axial depth of cut is 0.7 mm/z, the feed per tooth is 0.1 mm/z, and the spindle speeds are 1100 r/min, 1200 r/min, 1300 r/min, and 1400 r/min. Compared to the axial depth of cut and feed per tooth, the machining deformation of the housing changes less with the increase of the spindle speed. As shown in Figure 10(d), the deformation is larger when the number of clamping plates is 4 or 6, but decreases rapidly with the increase of the number of clamping plates. When the number of clamping plates is 8 or 10, the deformation continues to decrease but is very close to the expected value.

In summary, all three milling parameters have a certain impact on the machining deformation of the housing. To improve the machining accuracy of the housing, research should focus on these three factors. Furthermore, using 8 or 10 clamping plates can effectively reduce machining deformation during end milling of the casing. However, considering the time required to install the clamping plates and the efficiency and interference during casing machining, it is more appropriate to use 8 evenly distributed clamping plates for clamping.

4. Conclusion

(1) Based on the principle of end milling of thin-walled parts, and using the finite element method as the theoretical basis, a finite element simulation model for end milling of the outer ring belt of the casing was established using a Python-based ABAQUS secondary development platform. A method for predicting end milling deformation of casing parts based on quasi-statics was proposed, and experimental comparative analysis showed that the proposed prediction method has high accuracy.

(2) Using the established prediction model, the deformation of the casing end milling was analyzed. The results showed that the local geometric characteristics of the casing can affect

the local rigidity of the structure to a certain extent, leading to significant inconsistencies in the deformation of the ring belt. The consistency of local deformation must be considered in the formulation of the machining process.

(3) Using the established prediction model, the influence of milling process parameters and the number of clamping plates on the end milling deformation of the casing parts was analyzed. The results showed that there was a significant positive correlation between the component deformation and the milling process parameters, and the axial depth of cut was the most influential factor. However, there was a negative correlation between the component deformation and the number of clamping plates. When the number of clamping plates was greater than 8, its effect on suppressing the deformation of the casing tended to be gradual.

References

[1] AO Zhiqiang, WU Jianjun, WANG Zhongqi, et al. Study on the machining deformation by finite element method and experiment for typical thin-wall components using Abaqus[J]. Machine Tool & Hydraulics, 2007, 35(2):15-18.

[2] J. W. Sutherland, R. E. DeVor. An Improved Method for Cutting Force and Surface Error Prediction in Flexible End Milling Systems[J]. Journal of manufacturing science & engineering, 1986, 108 (4). 269-279.

[3] Lajzok M R. Study of some aspects of metal cutting-a three dimension finite element method[J]. Urbana： University of Illinois at Urbana-Chanpaign, 2016, 34(1):1-7.

[4] Erhan Budak, Yusuf Altintas. Modeling and avoidance of static form errors in peripheral milling of plates[J]. International Journal of Machine Tools & Manufacture, 1995, 35(3).459-476.

[5] Jian-Wei Ma, Ning Zhang, Si-Yu Chen, et al. Deformation analysing for thin-walled parts based on analysis of single-tooth or multi-tooth milling[J]. Int. J. of Machining and Machinability of Materials, 2018, 20(6).

[6] S. Ratchev, S. Liu, W. Huang, et al. Milling error prediction and compensation in machining of low-rigidity parts[J]. International Journal of Machine Tools and Manufacture, 2004, 44(15).

[7] Hua Bing Ouyang. Deformation prediction based on BP artificial neural network of milling thin-walled aluminum alloy parts[J]. Applied Mechanics and Materia.

[8] LIAO Kai, ZHANG Xiaodi, CHE Xingfei, et al. Construction and analysis of mechanical model forprocessing deformation of thin-walled aluminum alloy parts[J]. Journal of Harbin University of Technology, 2018, 50(05):166-172.

[9] LI Tong, TANG Aijun, ZHAO Yanhua, et al. Finite element simulation of cutting parameters on deformation law of curved thin-walled parts[J]. Manufacturing Automation, 2020, 42(04):47-50.

[10] Lou Wenming, Wu Jianjun, Kang Yonggang. Investigation on prediction method of surface deformation of thin-walled workpiece in peripheral milling[J]. Tool Engineering, 2007(05):40-44.

[11] YU Jin, WANG Yinqi. Machining deformation prediction of large curved thin-walled parts based on secondary development of ABAQUS[J]. Machine Tools and Hydraulic Pressure, 2018, 46(11):172-175.

[12] ZHANG Yu, LIAO Baoliang, QIN Zhenkun, et al. Deformation models and deformation research of milling thin walled parts[J]. Tool Engineering, 2017, 51(02):18-20.

[13] Jones A B. Ball motion and sliding friction in ball bearings[J]. Journal of Basic Engineering, 1959, 81(1):1-12.

[14] Ohta H, Sakaguchi T, Uchiumi M. Load-displacement relationship of a ball bearing with axial, radial, and angular displacements for both the inner and outer rings[J]. Journal of Tribology, 2017, 139:011103.

[15] Li Xiaohu, Li Huanfeng, Hong Jun, et al. Heat analysis of ball bearing under nonuniform preload based on five degrees of freedom quasi-static model[J]. Proceedings of the Institution of Mechanical Engineers, Part J: Journal of Engineering Tribology, 2016, 230(6):709-728.

[16] YU Dong, LI Xiaohu, ZHANG Jinhua, et al. Quasi statics model quick iteration method for RV reducer main bearing[J]. Journal of Xi'an Jiaotong University, 2016, 50(04):100-107.

[17] YU Jie, LIU Zhong, SHAO Juan, et al. Dynamic characteristics analysis of spindle bearing based on optimized quasi-static model[J]. Machine Tool & Hydraulics, 2020, 48(19):55-64.

[18] CHEN Yinglin, SHI Wenhua, CHEN Jiangyi,et al.Simplified analytical method for quasi-static model of main bearing for RV reducer[J]. Bearing, 2021, (04):12-17.

[19] GAO Feng, HE PingPing, LI Yan. Improved algorithm for quasi-static solution of high speed angular contact ball bearing[J]. Journal of Mechanical Strength, 2018, 40(03):613-619.

[20] Huang Zhigang, Ke Yinglin, Wang Litao. Study on related techniques for the finite element method simulation in metal cutting[J]. China Mechanical Engineering, 2003(10):42-45+4.

[21] LIU Weiwei, ZHU Lijian, YAO Changfeng, et al. Turning technology of GH4169 superalloy[J]. Aeronautical Manufacturing Technology, 2012(14):48-51.

[22] Liu Si-meng, Shao Xiao-dong, Ge Xiao-bo, et al. Simulation of the deformation caused by the machining cutting force on thin-walled deep cavity parts[J]. The International Journal of Advanced Manufacturing Technology, 2017, 92(9-12).

[23] FAN Xiaoliang, WU Xuehua, WANG Jinfeng, et al. Numerical simulation and experiment in high-speed cutting superalloy GH4169[J]. Journal of Beijing University of Aeronautics and Astronautics, 2016, 42(07):1344-1351.

[24] WANG Guangyu, WU Yunxin, YAN Pengfei, et al. Prediction model for machining deformation of aeronautical aluminum alloy thin-walled workpiece[J]. Journal of Central South University(Science and Technology), 2012, 43(05):1696-1702.